Supplement of

Representing dynamic grass density in the land surface model ORCHIDEE r9010

Siqing Xu[1,2], Sebastiaan Luyssaert[3], Yves Balkanski[1], Philippe Ciais[1,2], Nicolas Viovy[1], Liang Wan[4], Jean Sciare[2]

[1]Laboratoire des Sciences du Climat et de l'Environnement (LSCE), CEA-CNRS-UVSQ, Gif-sur-Yvette, France

[2]The Cyprus Institute, Climate and Atmosphere Research Center (CARE-C), Nicosia, Cyprus

[3]Amsterdam Institute for Life and Environment, Department of Ecological Science, Vrije Universiteit Amsterdam, Amsterdam, The Netherlands

[4]Research Institute of Agriculture and Life Sciences, Seoul National University, Seoul, Republic of Korea

Correspondence to: Siqing Xu (siqing.xu@lsce.ipsl.fr)

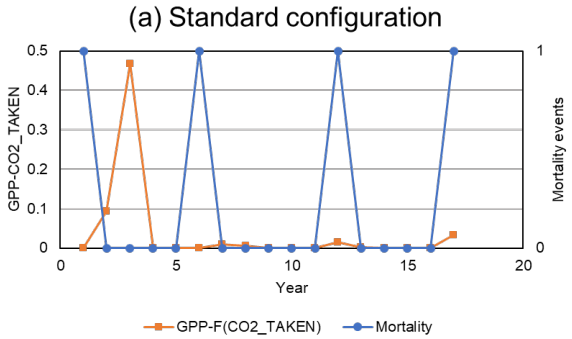

Figure S1. Temporal dynamics of productivity (GPP – F_{CO2_TAKEN}, orange, left axis) and mortality events (blue, right axis) at (59° E, 39° N) in the fixed maximum density approach over 17 years. Subtracting F_{CO2_TAKEN} from GPP (gross primary productivity) is intended to remove the artificial carbon uptake from the atmosphere.

15

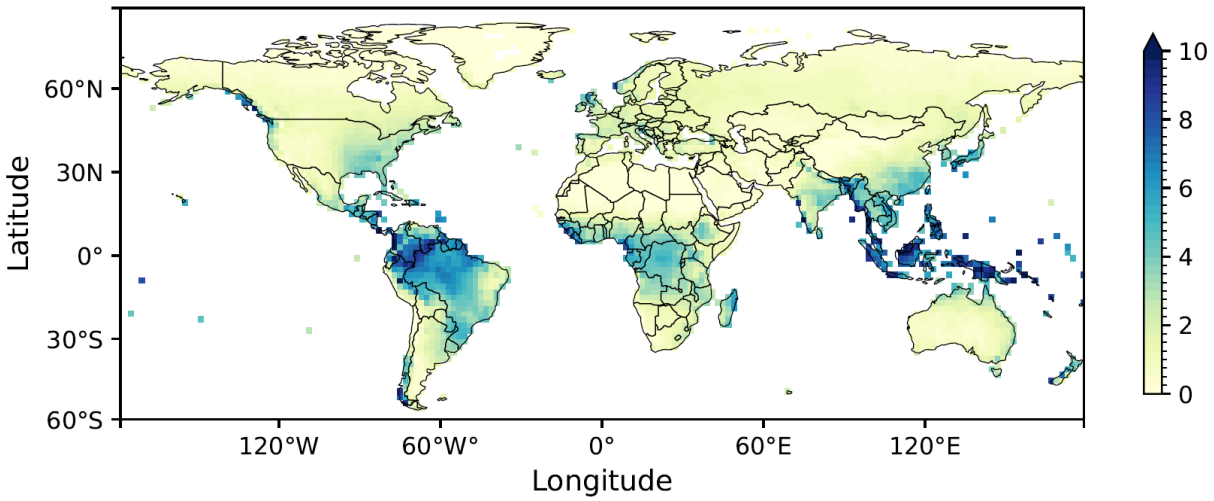

Figure S2. Global map of annual rainfall rate (mm per day) averaged over 17 years (2004-2020). The rainfall data is derived from CRU-JRA dataset as the input data.

	a	b	c	d
Water stress	Linear (by default)	Linear(by default)	Exponential, alpha=8	Exponential, alpha=8
Target of reserve + labile	(by default)	Multiply by 1.5 times	(by default)	Multiply by 1.5 times

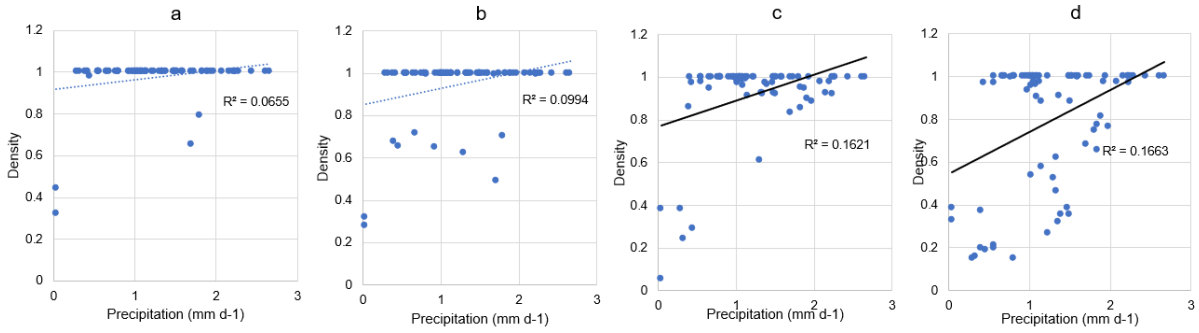

Figure S3. Regression between precipitation and grass density for C_4 grasslands in Southern Africa. The coefficient of determination (R^2) increases progressively from (a) to (d):

(a) uses the default water stress function for transpiration and the default targets for reserve and labile carbon;

(b) applies the higher targets for reserve and labile carbon while keeping the default water stress function;

(c) uses an exponential function for water stress but retains the default targets for reserve and labile carbon;

(d) combines both the exponential water stress function and the higher targets for reserve and labile carbon.

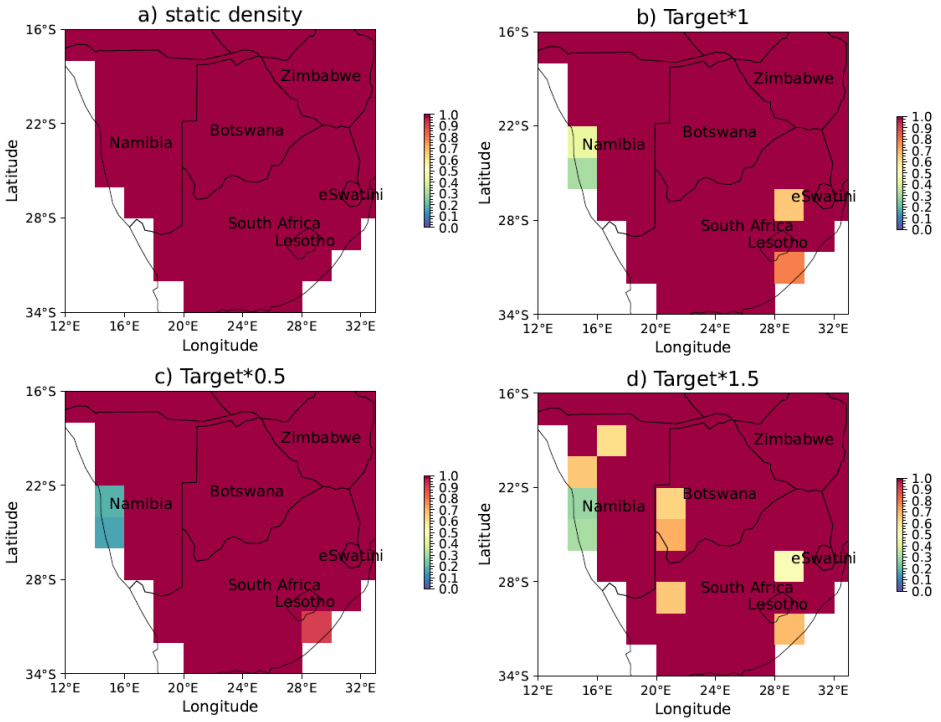

Figure S4. Grass density in C_4 grasslands averaged from 2004 to 2020 in the fixed maximum density (a) and dynamic density approach (b–d). For C_4 grasslands, the target for reserve and labile carbon was multiplied by a scaling factor, with value 1 (b), 0.5 (c) and 1.5 (d).

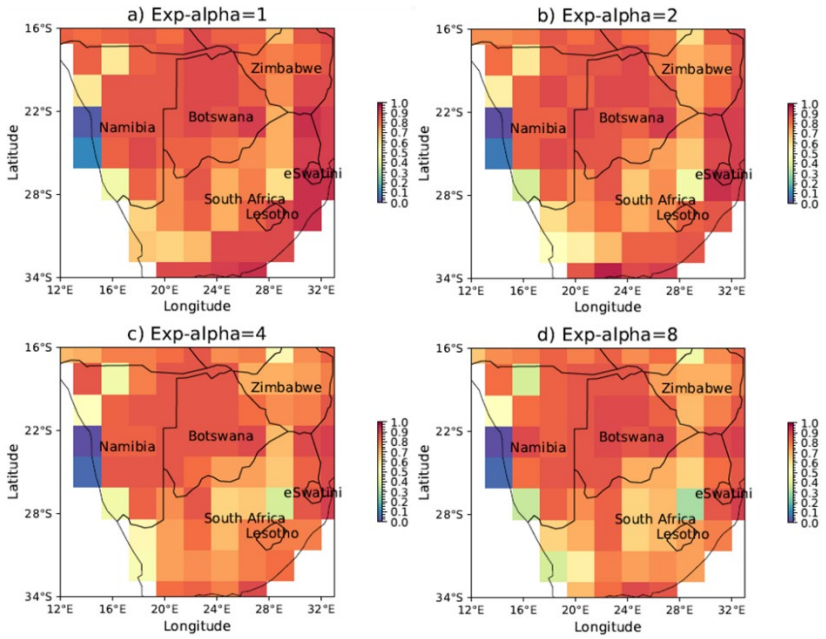

Figure S5. Grass density in C_4 grasslands averaged from 2004 to 2020 in the dynamic density approach with different parameters in the exponential water stress function over Southern Africa. The parameters in water stress of transpiration were set to 1 (a), 2 (b), 4 (c) and 8 (d).

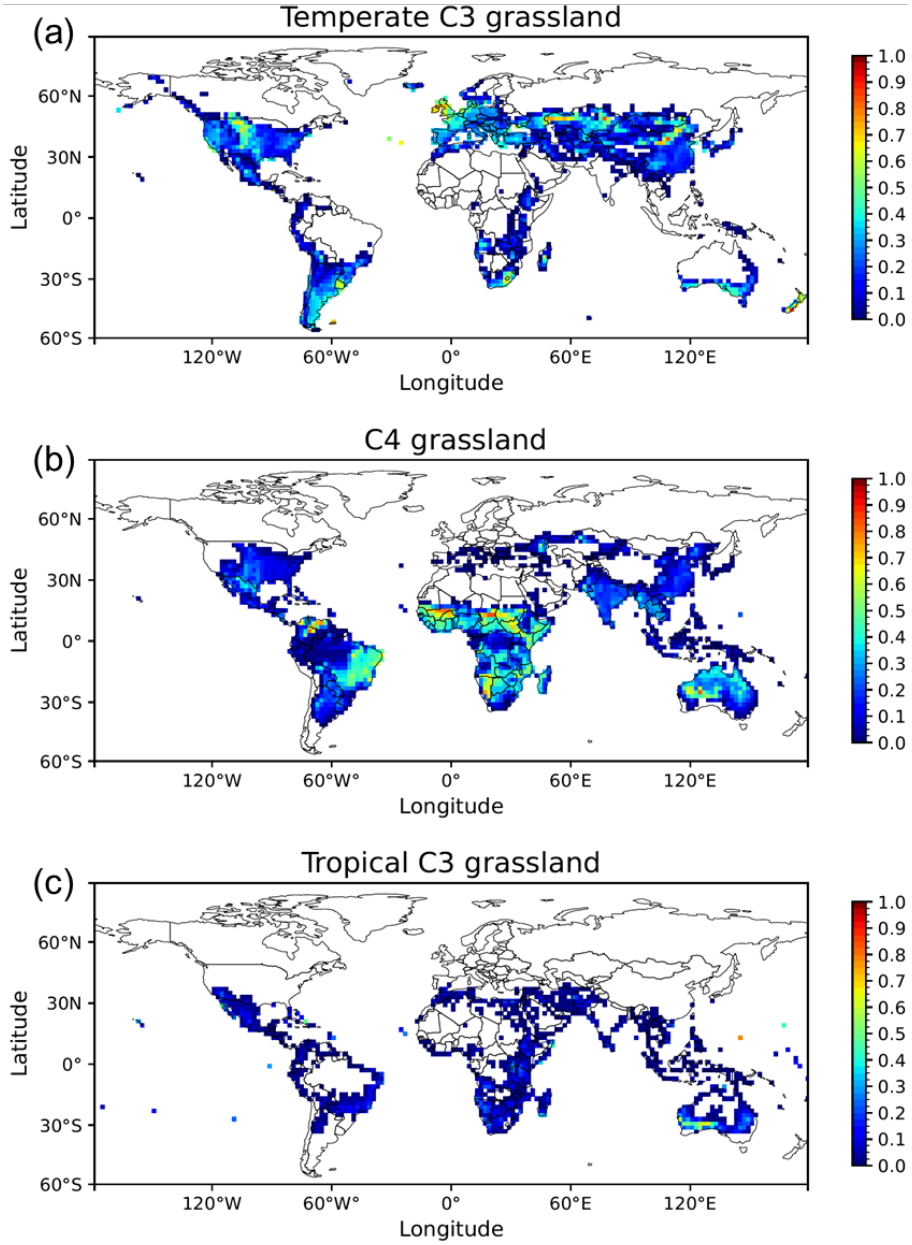

Figure S6. The global land cover map of grassland PFTs in 2004. The map was derived from the ESA CCI Land Cover dataset (Poulter et al., 2015; ESA, 2017) and used as a fixed input for all ORCHIDEE simulations.

25

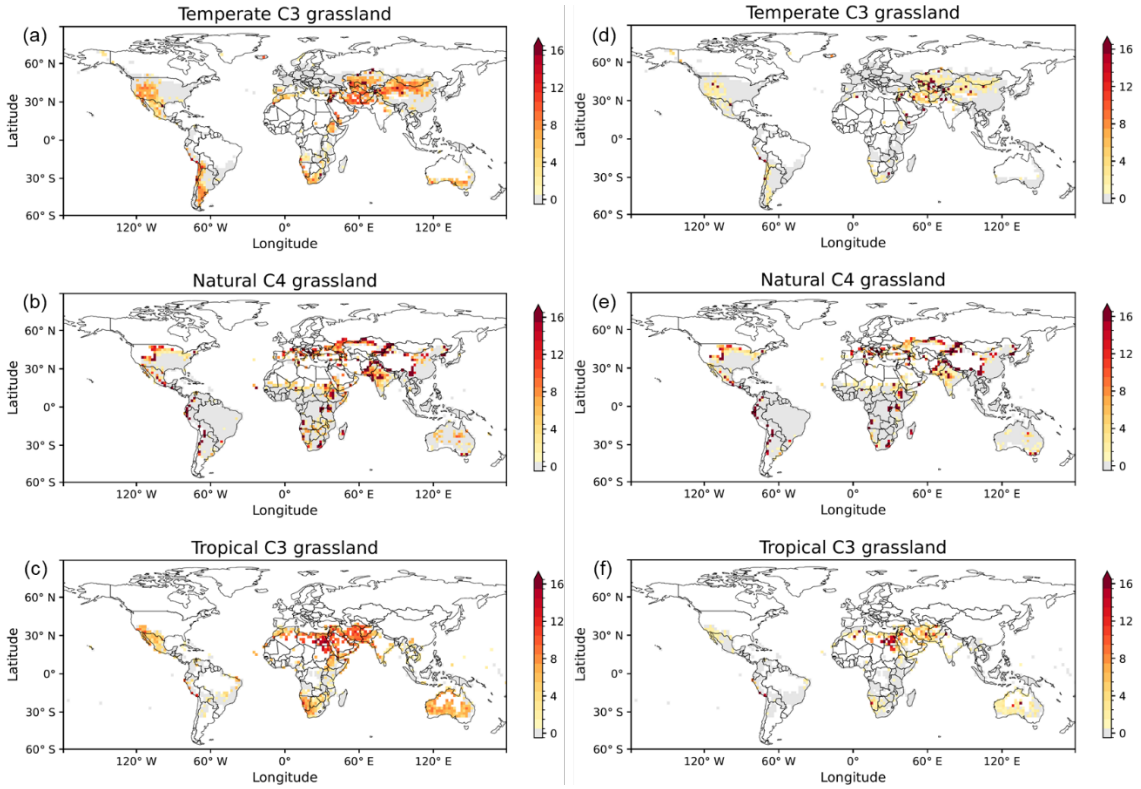

Figure S7. Frequency of individual productivity falling below the critical threshold of 10^{-4} gC per individual. Individual productivity is calculated as (GPP – $F_{CO_2\_TAKEN}$) divided by grass density, where $F_{CO_2\_TAKEN}$ refers to the artificial carbon uptake from the atmosphere. The figure shows the number of years in which productivity falls below the survival threshold, indicating conditions insufficient to support vegetation persistence, over a 17-year period. Results are shown for three grassland types under the fixed density approach (a–c) and the dynamic density approach (d–f).

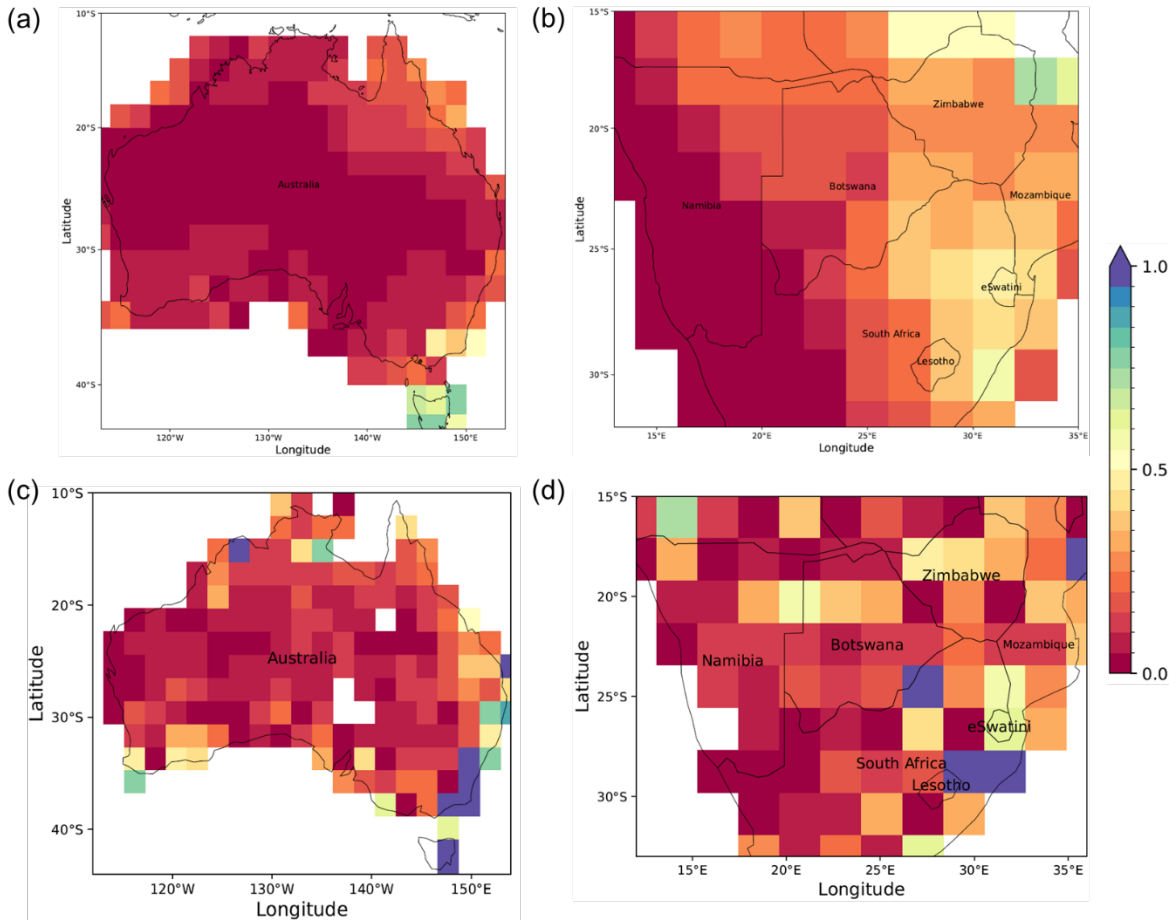

Figure S8. Mean annual LAI in grasslands in 2019 derived from the Sentinel-2 dataset and ORCHIDEE using the dynamic density approach in Australia and Southern Africa. The Sentinel-2 data, initially at a 10 m resolution, has been aggregated to a 2° × 2° grid for analysis over Australia (a) and Southern Africa (b). For comparison, mean annual LAI values simulated from ORCHIDEE with the dynamic density approach in 2019 are also shown for Australia (c) and Southern Africa (d).